

Rotor flux oriented control of induction machine based drives with compensation for the variation of all machine parameters

G. EXTREMIANA¹, G. ABAD^{2*}, J. ARZA¹, J. CHIVITE-ZABALZA¹, and I. TORRE¹

¹ Ingeteam Power Technology S. A., Parque Tecnológico de Bizkaia, Edificio 110, 48170 Zamudio – Spain

² The University of Mondragon, Loramendi 4 Aptdo 23, 20500 Mondragon, Spain

Abstract. The performance of rotor flux oriented induction motor drives, widely used these days, relies on the accurate knowledge of key machine parameters. In most industrial drives, the rotor resistance, subject to temperature variations, is estimated on-line due to its significant influence on the control behaviour. However, the rest of the model parameters are also subject to slow variations, determined mainly by the operating point of the machine, compromising the dynamic performance and the accuracy of the torque estimation.

This paper presents an improved rotor-resistance on-line estimation algorithm that contemplates the iron losses of the electrical machine, the iron saturation curve and the mechanical losses. In addition, the control also compensates the rest of the key machine parameters such as the leakage and magnetizing inductances and the iron losses. These parameters are measured by an off-line estimation procedure and stored in look up-tables used by the control. The paper begins by presenting the machine model and the proposed rotor flux oriented control strategy. Subsequently, the off-line parameter measurement procedure is described. Finally, the algorithm is extensively evaluated and validated experimentally on a 15 kW test bench.

Key words: parameter on-line estimation, rotor flux oriented control, magnetizing curve, iron losses.

1. Introduction

Induction motor drives are nowadays the most popular type of electrical machine in the field of high performance motor drives, thanks to the development of Flux Oriented Control (FOC) techniques [1–3]. The work presented in this paper was originally aimed at drives of any output power, ranging from a few dozens of kW to 4 MW in the case of low voltage drives, up to powers of tens of MW in the case of medium voltage drives. These find applications in the industrial, e.g. paper and steel mills; marine, e.g. propulsion systems and pumps; railway traction and wind generation markets [4–6].

The Rotor Flux Oriented Control (RFOC) is perhaps the most widely used Flux Oriented Control (FOC) strategy in industry. They are used in applications covering all power ranges. However, alternative control techniques such as Direct Torque Control (DTC) or Direct Self-Control (DSC) are also well used and researched [7–11], including those using multilevel converter-fed drives.

FOC induction motor drives require a good flux orientation for a correct torque estimation and to make use of all the available power. This is of paramount importance in applications that receive a torque setpoint, such that web processes (e.g. paper/steel mills and winders) and traction applications, which typically require a torque accuracy of 1% to 3%. Even for applications that receive a speed setpoint, a detuned drive will exhibit a degraded performance and can demand more voltage and current than necessary [12], impairing the maximum achievable torque and power. The rotor flux orientation relies upon the accurate knowledge of some key machine parameters such as the magnetizing inductance, the stator and

rotor leakage inductances and the rotor resistance. The magnetizing inductance, and to a less extent, the rotor leakage [13–14], are affected by saturation. The rotor resistance is primarily affected by temperature variations, but it could also vary with the slip frequency [15]. In addition, there are parameters often neglected in the basic machine model, such as the core losses and the mechanical losses of the machine, which are an additional source of errors. The former varies with flux levels and frequency and the latter with the rotor speed.

A comprehensive review on the parameter estimation techniques for induction motor RFOC drives, out of the scope of this paper can be found in the literature [16–19]. In practice, commercial motor drives usually provide online compensation for the saturation of the magnetizing inductance and the temperature drift of the rotor resistance. The former is typically based on a Look Up Table (LUT), generated by taking offline measurements, ideally by freely rotating the motor unloaded [20–22]. The latter is usually estimated online by employing a Model Reference Adaptive System (MRAS) approach, based on the calculation of the reactive power. This method, usually disabled for low values of slip, has a slow dynamic response and achieves good steady-state orientation, often at the expense of obtaining an incorrect value of rotor resistance as it tries to compensate errors incurred by other model parameters.

On the other hand, in [23–25], an alternative flux orientation is investigated, based on the stator flux estimation by means of the stator voltage model. This approach eliminates the dependence on the rotor resistance; however, the stator resistance identification and an accurate knowledge of the volt-

*e-mail: gabad@mondragon.edu

age drop in the inverter switching devices are required with this philosophy. Finally, [26] is an example of reference which proposes the estimation methods of machine parameters and mechanical systems including non-linear effects by means of advanced control and estimation theory methods. Then, [27] for instance in a slightly different approach, estimates the parameters of the machine at standstill, reducing the number of sensors needed.

Therefore, this paper presents an improved control algorithm, based on a simple machine model that contemplates the iron losses, in the shape of a loss equivalent resistor, which also includes the mechanical losses. In addition, the online rotor resistance estimation MRAS algorithm has been adapted to this new machine model. Moreover, the saturation of the magnetizing inductance is also included, based on the calculation of the air-gap flux producing current. One of the merits of the proposed control strategy, as opposed to other more sophisticated ones relies on its simplicity, making it straightforward to implemented by most industrial companies. In addition to this, an extensive experimental evaluation is provided at the end of the paper, covering several practical cases from a drive manufacturer point of view, demonstrating the effectiveness of the proposed control and parameter compensation approach.

2. Dynamic model of the induction machine considering the iron losses

Traditional models of the Induction Machine (IM) do not take into account the core losses that may be present in the machine. These depend on factors such as constructive criteria, power ranges, etc. In some occasions, the iron losses may be significant and should not be neglected for a proper and accurate modeling. Hence in this section, the $\alpha\beta$ model of the IM is developed considering the iron losses.

$\alpha\beta$ Dynamic Model Equations. The model of the IM is developed using the space vector representation in the stator reference frame and considering the iron losses [20–22]. The voltage equations are the same as those used in traditional IM models:

$$\vec{v}_s^s = R_s \cdot \vec{i}_s^s + \frac{d\vec{\psi}_s^s}{dt}, \quad (1)$$

$$0 = R_r \cdot \vec{i}_r^s + \frac{d\vec{\psi}_r^s}{dt} - j \cdot \omega_m \cdot \vec{\psi}_r^s, \quad (2)$$

with \vec{v}_s^s being the stator voltage space vector, \vec{i}_s^s , \vec{i}_r^s the stator and rotor current space vectors and $\vec{\psi}_s^s$, $\vec{\psi}_r^s$ the stator and rotor flux space vectors. On the other hand, R_s , R_r are the stator and rotor resistances and ω_m the angular speed of the shaft.

Similarly, the flux equations can be expressed as follows:

$$\vec{\psi}_s^s = L_{\sigma s} \cdot \vec{i}_s^s + L_h \cdot \vec{i}_h^s, \quad (3)$$

$$\vec{\psi}_r^s = L_h \cdot \vec{i}_h^s + L_{\sigma r} \cdot \vec{i}_r^s, \quad (4)$$

with $L_{\sigma s}$ and $L_{\sigma r}$ being the leakage inductances, L_h the mutual inductance and \vec{i}_h^s the mutual current. Note that only part of the rotor and stator currents are responsible of the flux creation. Then, the mutual circuit equations are described as:

$$\vec{i}_s^s + \vec{i}_r^s = \vec{i}_{fe}^s + \vec{i}_h^s, \quad (5)$$

$$R_{fe} \cdot \vec{i}_{fe}^s = L_h \cdot \frac{d\vec{i}_h^s}{dt}, \quad (6)$$

where R_{fe} and \vec{i}_{fe}^s are the iron loss resistance and current respectively. Finally, the torque equation is defined as:

$$T_{em} = \frac{3}{2} \cdot p \cdot \text{Im} \left\{ \vec{\psi}_r^s \cdot \vec{i}_r^{*s} \right\}. \quad (7)$$

Consequently, a dynamic model for a IM that takes into account the iron losses can be defined by using Eqs. (1)–(7). That model can be expressed in a graphical format by means of the two equivalent circuits of Fig. 1, which are based on the α and β stationary reference frames respectively.

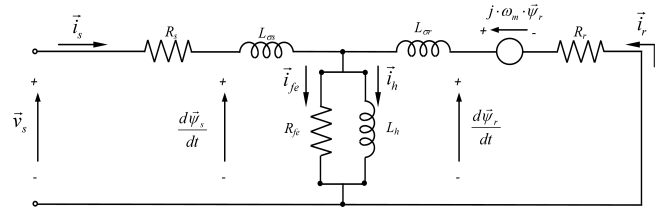


Fig. 1. $\alpha\beta$ model of the IM in stator coordinates considering the iron losses

2.1. Steady-state equivalent circuit and variation of the machine parameters for different points of operation.

A simplified steady-state IM model can be easily obtained from the dynamic model of the IM shown in Fig. 1 [15]. That model, presented in Fig. 2 using a phasor notation, shows the dependence of the various machine parameters on variables that change for the different operating conditions. For instance, the rotor resistance is not constant and depends on the angular speed of the rotor voltages and currents ω_r and on the operating temperature. Similarly, the rotor leakage inductance depends on ω_r and the rotor current amplitude, while the stator leakage inductance depends on the stator current amplitude and ω_s , the angular frequency of stator currents and voltages.

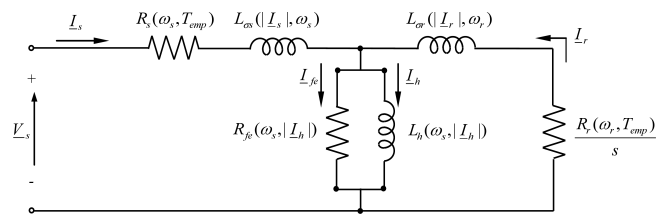


Fig. 2. Single phase equivalent steady-state circuit of the IM, considering variable parameters as function of the operating conditions

As it is explained later on in this paper, the machine parameters can be estimated off-line for different operating points.

3. Vector control strategy

Vector control strategies for AC machines have been actively researched by many authors and manufacturers among the years. From the basic control principle and structure firstly proposed by [1], we can find a wide range of variants of vector control. In this research work, the basic vector control

structure [2] has been enhanced by including the iron losses present in the IM.

3.1. Vector control structure considering iron losses. RFOC vector control is based on the dq reference frame being aligned with the rotor-flux space vector of the machine, as shown in Fig. 3. In doing so, Eqs. (1)–(7) can be manipulated to allow an easy and straightforward representation of the induction machine that is suitable for control purposes.

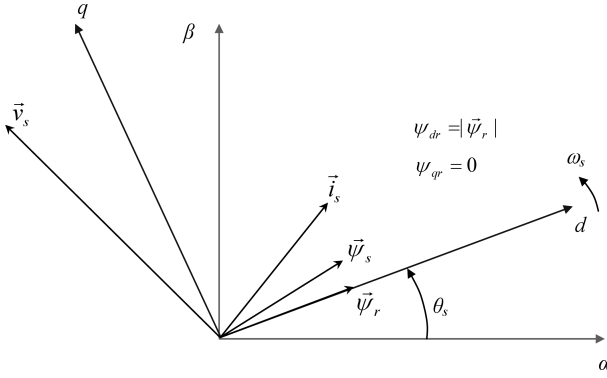


Fig. 3. Alignment with rotor flux in Vector Control Strategy

The rotor flux space vector can be expressed in function of the stator and rotor currents as follows:

$$\begin{aligned} \frac{d\vec{\psi}_r}{dt} \left(1 + \frac{R_{fe}L_r}{R_rL_h} + j\frac{\omega_sL_{\sigma r}}{R_r} \right) \\ - \vec{\psi}_r \left(\frac{\omega_r\omega_sL_{\sigma r}}{R_r} - \frac{R_{fe}}{L_h} - j\frac{\omega_rR_{fe}L_r}{R_rL_h} - j\omega_s \right) \\ - R_{fe}\vec{i}_s - L_{\sigma r}\frac{d\vec{i}_r}{dt} = 0. \end{aligned} \quad (8)$$

Taking the d component of this expression and assuming that it the d axis is perfectly aligned with the rotor flux space vector the following expression is obtained:

$$\begin{aligned} \frac{d|\vec{\psi}_r|}{dt} \left(\frac{1}{R_{fe}} + \frac{L_r}{R_rL_h} \right) - |\vec{\psi}_r| \left(\frac{\omega_r\omega_sL_{\sigma r}}{R_{fe}R_r} - \frac{1}{L_h} \right) \\ - i_{ds} - \frac{L_{\sigma r}}{R_{fe}} \frac{di_{dr}}{dt} = 0. \end{aligned} \quad (9)$$

By looking at the expression it can be seen how the rotor flux amplitude is due to the d component of stator current (i_{ds}). On the other hand, by manipulating in dq reference frame expressions (1) to (8), the torque at steady-state can be represented as follows:

$$T_{em} = \frac{3}{2} \frac{p}{R_r \left(\frac{1}{R_{fe}} + \frac{L_r}{R_rL_h} \right)} \left(|\vec{\psi}_r| i_{qs} - \frac{\omega_m |\vec{\psi}_r|^2}{R_{fe}} \right). \quad (10)$$

Which means that the torque is mainly produced by the q component of stator current (i_{qs}).

Finally, dq stator voltage equations can be also derived by following the same procedure, yielding:

$$\begin{aligned} v_{ds} = i_{ds} (R_s + R_{fe}) - \omega_s L_{\sigma s} i_{qs} - \frac{R_{fe}}{L_h} |\vec{\psi}_r| \\ - \frac{R_{fe}L_r}{R_rL_h} \frac{d|\vec{\psi}_r|}{dt} + L_{\sigma s} \frac{di_{ds}}{dt}, \end{aligned} \quad (11)$$

$$\begin{aligned} v_{qs} = i_{qs} (R_s + R_{fe}) + \omega_s L_{\sigma s} i_{ds} \\ - \frac{R_{fe}L_r}{R_rL_h} \omega_r |\vec{\psi}_r| + L_{\sigma s} \frac{di_{qs}}{dt}. \end{aligned} \quad (12)$$

Notice that d and q components of stator voltage-currents are coupled, but can be independently produced employing basic vector control theory [1].

Therefore, the control block diagram of Fig. 4, presents the proposed basic vector control structure based on Eqs. (9)–(12). It comprises a pair of two nested control loops, totaling four control loops. These loops are responsible for producing the switching signals to the semiconductor devices of the converter, as they aim to follow the rotor flux amplitude and speed references. In order to achieve this, the control loops require the estimation of certain key non-measurable machine variables. If a good accuracy in the flux control is required, together with a good knowledge of the torque, the estimation block of Fig. 4 should also consider the variation of key machine parameters for different operating points as seen in Sec. 3. The next subsection presents a set of different estimation techniques available that serve this purpose.

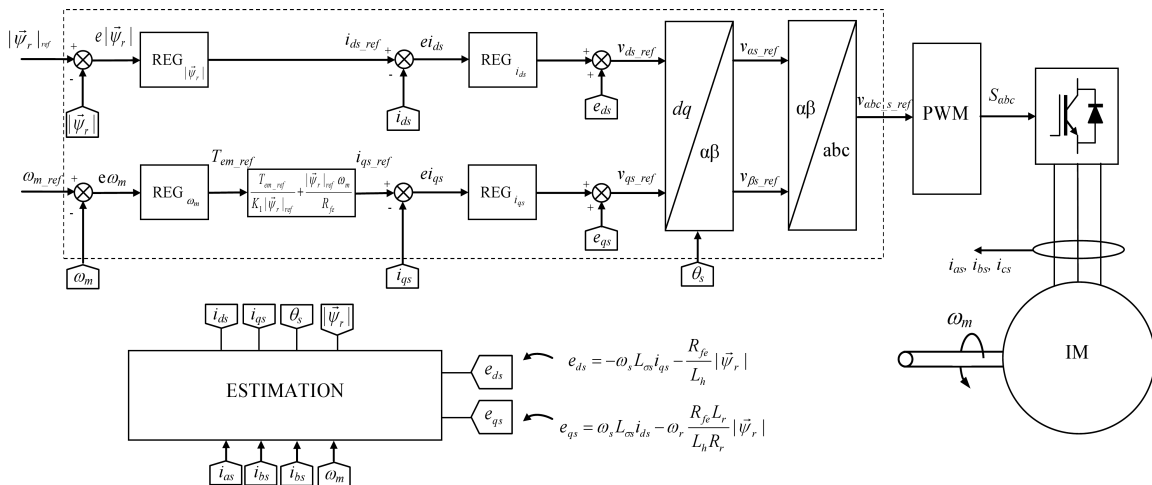


Fig. 4. Vector control of the squirrel cage induction machine considering the iron losses

3.2. Estimation of the rotor flux. The first non-measurable magnitude that must be estimated is the rotor flux amplitude. From Eq. (9), by applying the Laplace transformation and neglecting the rotor current term, the rotor flux amplitude yields:

$$|\vec{\psi}_r|(s) = \frac{i_{ds}(s)}{\left(\frac{1}{R_{fe}} + \frac{L_r}{R_r L_h}\right) s + \left(\frac{1}{L_h} - \frac{\omega_r \omega_s L_{\sigma r}}{R_r R_{fe}}\right)}. \quad (13)$$

Assuming a good orientation of the d axis of the synchronous reference frame to the rotor flux space vector, the rotor flux amplitude can be simply estimated by using the d component of the stator current, the rotor speed, the supply frequency and a few parameters of the machine, which may vary depending on the operating point. The block diagram of this estimator is depicted in Fig. 9.

3.3. Estimation of ω_r . Since the RFOC vector control is based on the alignment of the d axis of the synchronous reference frame to the rotor flux space vector, it is of paramount importance to accurately estimate the rotor slip speed ω_r . Again, by looking at Eq. (8) and by taking into account the q -axis component, the following expression is obtained:

$$\omega_r = \frac{i_{qs} - \frac{\omega_m \cdot |\vec{\psi}_r|}{R_{fe}}}{\left(\frac{1}{R_{fe}} + \frac{L_r}{R_r \cdot L_h}\right) \cdot |\vec{\psi}_r|}. \quad (14)$$

It can be noticed, how the slip speed depends again on several key machine parameters, the rotor flux and i_{qs} . The inclusion of the iron losses in the control has a clear effect on the main vector control magnitudes $|\vec{\psi}_r|$ and ω_r . Moreover, since the parameter R_{fe} is present in both equation (9) and (10), a cross-coupling appears between the coupled dependence of the rotor flux from i_{qs} (through ω_r), and also a coupled dependence of the slip speed from i_{ds} (through $|\vec{\psi}_r|$).

If the machine's iron losses are very low, the R_{fe} takes a very high value and expressions (8) and (9) become those used in classic vector control theory:

$$\frac{|\vec{\psi}_r|(s)}{i_{ds}(s)} = \frac{L_h}{R_r s + 1}, \quad \omega_r = \frac{R_r \cdot i_{qs}}{L_h \cdot |\vec{\psi}_r|}. \quad (15)$$

Under these circumstances, the rotor flux orientation achieves total decoupling from stator i_{ds} and i_{qs} currents. The slip estimation as well as the angle calculation block diagrams when the iron losses are considered are illustrated in Fig. 9.

It must be highlighted, that in order to achieve accurate estimation of $|\vec{\psi}_r|$ and ω_r with Eqs. (13) and (14), it is very important to well know the values of all machine parameters, which in most of the cases, they are modified depending on the operation point of the machine. For that purpose, the on-line estimation procedure described in subsequent sections is proposed and evaluated. Note also that the dq reference frame based estimation of indirect vector control [2, 3, 22], is well suited to avoid problems due to drift of integrators in measured currents of other estimation philosophies ($\alpha\beta$ reference frame based for instance), even at very low speeds.

3.4. Estimation of the magnetizing inductance. As reported by many authors [15, 20], the mutual inductance value depends on the mutual current amplitude $|\vec{i}_h|$. Therefore, mainly if the machine is to operate in the flux weakening range, it is necessary to on-line estimate the L_h value during operation. Consequently, by manipulating expressions (2)–(6), the mutual dq currents can be expressed as follows:

$$i_{dh} = i_{ds} + \omega_r \omega_s |\vec{\psi}_r| \frac{L_{\sigma r}}{R_r R_{fe}}, \quad (16)$$

$$i_{qh} = i_{qs} - |\vec{\psi}_r| \left(\frac{\omega_r}{R_r} + \frac{\omega_s}{R_{fe}}\right). \quad (17)$$

Note that the R_{fe} term is also present, producing a coupling dependence of the currents on $|\vec{\psi}_r|$ and ω_r . Consequently, by knowing the mutual inductance current amplitude, the actual L_h value can be estimated as illustrated in the block diagram of Fig. 5. It simply requires the estimation of the current i_h flowing through the inductance in an open loop manner. Note that the variation of the mutual inductance with respect to the current, $L_h = f(|\vec{i}_h|)$, has to be measured off-line for the specific machine used, as described later in Subsec. 4.3. The dependence of L_h on ω_s has considered to be negligible for the usual supply frequency range of IM and has not been considered in this paper.

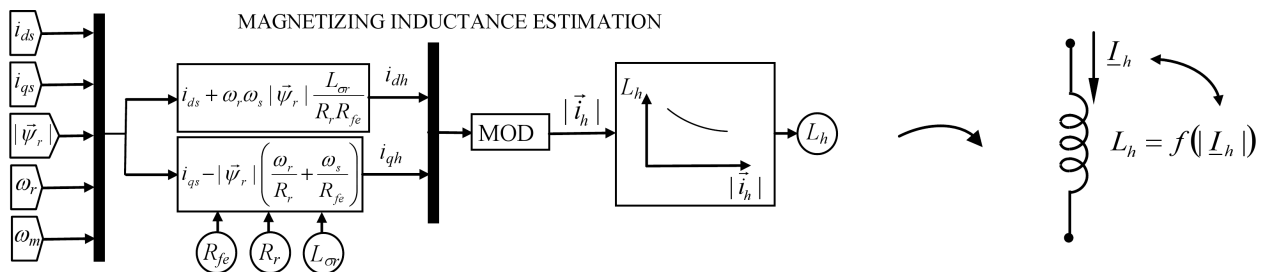


Fig. 5. Open loop magnetizing inductance estimation block diagram

3.5. Iron Losses Estimation. Iron losses, are difficult to calculate and they even require the use of finite element techniques for an accurate estimation. Although complex expressions have been found in the literature, Eq. (18) provides an approximation that is valid for a qualitative explanation [22].

$$P_{fe} = a f \hat{B}^2 + b (\Delta f \hat{B})^2, \quad (18)$$

where a and b depend on the material properties and Δ is the lamination thickness.

They are due to hysteresis and eddy current losses. Both are proportional to the square of the peak flux density. Hysteresis losses are proportional to the frequency whereas eddy losses are proportional to the square of the frequency. Since hysteresis losses are usually predominant, the iron losses will increase with the rotor speed in the constant torque region, and will decrease for speeds above rated in the field weakening region.

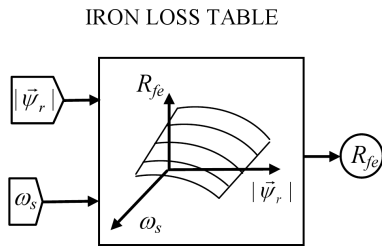


Fig. 6. Look-up table for R_{fe} adaptation on-line

As explained later on in Subsec. 4.3, it is difficult to separate the iron losses from the mechanical losses from the measurements obtained in a standard no-load test. The mechanical losses comprise a series of friction terms that can take a fixed value, such that the Coulomb friction, can be proportional to the rotor speed, such as the viscous friction, or can even be proportional to the square of the rotor speed, as is the case of the windage losses. In any case, once that steady-state operation has been reached they take a fixed value for a given supply frequency, just as well as the iron losses. For that reason, this paper takes the novel approach of considering them with the iron losses. That is, the iron-loss equivalent resistance depicted in the models of Fig. 1 and Fig. 2 represents both the mechanical and the iron losses and is on-line adapted,

according to the pre-calculated look-up table of Fig. 6 (how the table is obtained is explained in Subsec. 4.3). This approach is justified since the value of that iron-loss equivalent resistance is updated from a look-up table that is stored for several values of supply frequency and flux. The experimental results presented subsequently in this paper confirm the correctness of the approach.

3.6. Estimation of the rotor resistance. As reported in the literature [23, 24], the rotor and stator resistances values vary with temperature. Given the strong influence that the rotor resistance value has on the performance of the vector control strategy, as seen in (13)–(15), its value is usually estimated on-line, that is, during machine operation. In this paper, the rotor resistance is estimated based on stator reactive power computations, performed by two different expressions as defined in MRAS theory [16]. Thus, one reactive power computation is done directly from voltages and currents, while the other is IM model dependent. The first stator reactive power can be calculated by using the classical expression (reference model):

$$Q_s = 1.5 \cdot (v_{qs}i_{ds} - v_{ds}i_{qs}). \quad (19)$$

The stator currents are directly measured in real application, while the stator voltages can be obtained from their reference values or by voltage sensors. On the other hand, by manipulating expressions (1)–(6) and (12), it is possible to derive the following stator reactive power expression model dependent (adaptive model):

$$Q_s = 1.5 \cdot \left(L_{\sigma s} \omega_s |\vec{i}_s|^2 + \omega_s |\vec{\psi}_r| \left(\frac{L_{\sigma r}}{R_r} \omega_r i_{qs} + i_{ds} \right) \right). \quad (20)$$

It is important to notice that this expression shows a strong dependence on the machine parameter R_r at high torques (i_{qs}). Hence, a deviation on its actual value causes a deviation on the reactive power calculated according to expressions (19) and (20). This fact is used by the on-line resistance estimation block diagram shown in Fig. 7 based on MRAS theory.

It must be pointed out that, although to a less extent than R_r , other parameters such that R_{fe} , $L_{\sigma s}$, $L_{\sigma r}$ and L_h can also produce a stator reactive power error due to the presence of $|\vec{\psi}_r|$ and ω_r terms on expression (19). Consequently, it is important to know their values with good accuracy.

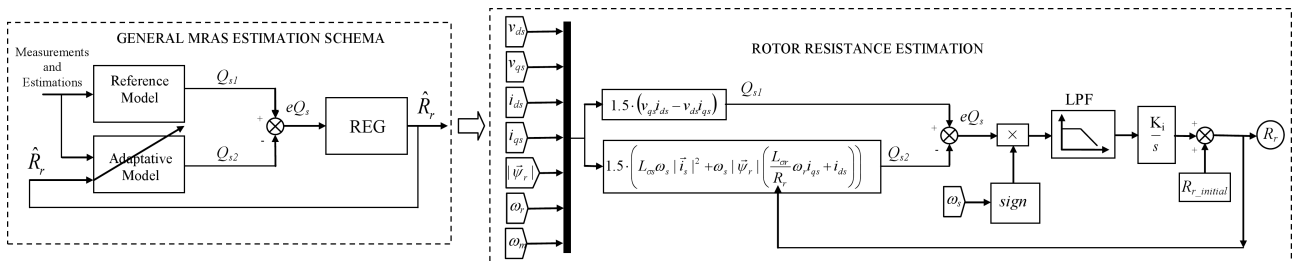


Fig. 7. R_r estimation based on MRAS theory, by means of reactive power error

Compared with the previous estimators, i.e., the mutual inductance and the iron loss resistance estimation, the rotor resistance estimation considers a non-modeled effect that is the rotor temperature, which cannot be easily included in an off-line table. However, the on-line L_h and R_{fe} estimated values are taken from fixed values stored in a table that has been previously off-line estimated. On the other hand, the dynamic performance of the R_r estimator can be modified by means of constant K_i . The analytical selection of this gain is out of the scope of this paper, however, the experimental validation presented in subsequent sections shows how it can be tuned experimentally.

Finally, it must be pointed out that this proposed R_r estimation method, compared with previously proposed alternative methods in literature, includes the R_{fe} dependence in the model based Q_s computation of expression (20) and can operate with the rest of the estimators proposed. This fact yields to successful and accurate results, as demonstrated in experimental and simulation validations shown in subsequent sections.

3.7. Leakage inductances estimation. In general, it could occur that leakage inductance values vary significantly depending on the operating point (stator and rotor currents mainly) of the machine [13–14]. In order to avoid accuracy problems in the estimators, this variation can also be considered at the control stage with the same philosophy as with the magnetizing inductance.

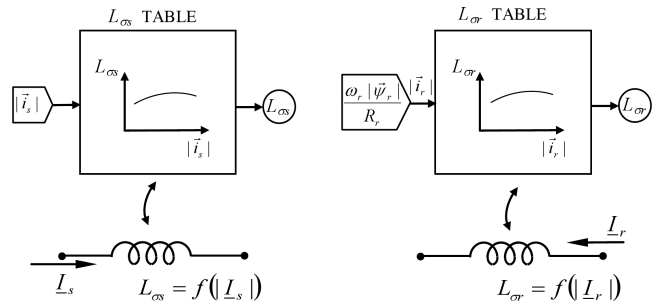


Fig. 8. Look-up tables for leakage inductance adaptation on-line

Figure 9 illustrates that both leakage inductances can be also obtained during control of the machine, from an off-line estimated table (the off-line estimation procedure is described in next section). L_{σ_s} can be directly obtained from stator current measurement, however, L_{σ_r} requires a rotor current estimation also, which comes from expression (2) transformed to synchronous rotating dq frame and assuming steady-state:

$$|\vec{i}_r| = \frac{\omega_r}{R_r} \cdot |\vec{\psi}_r|. \quad (21)$$

Finally, Fig. 9 illustrates the overall estimation block diagram structure. Note that L_{σ_r} affects in more estimators than L_{σ_s} . Nevertheless, unlike in the case of machines designed for line-start applications, in most machines designed for converter-fed drive applications, the leakage inductance terms do not present significant variations.

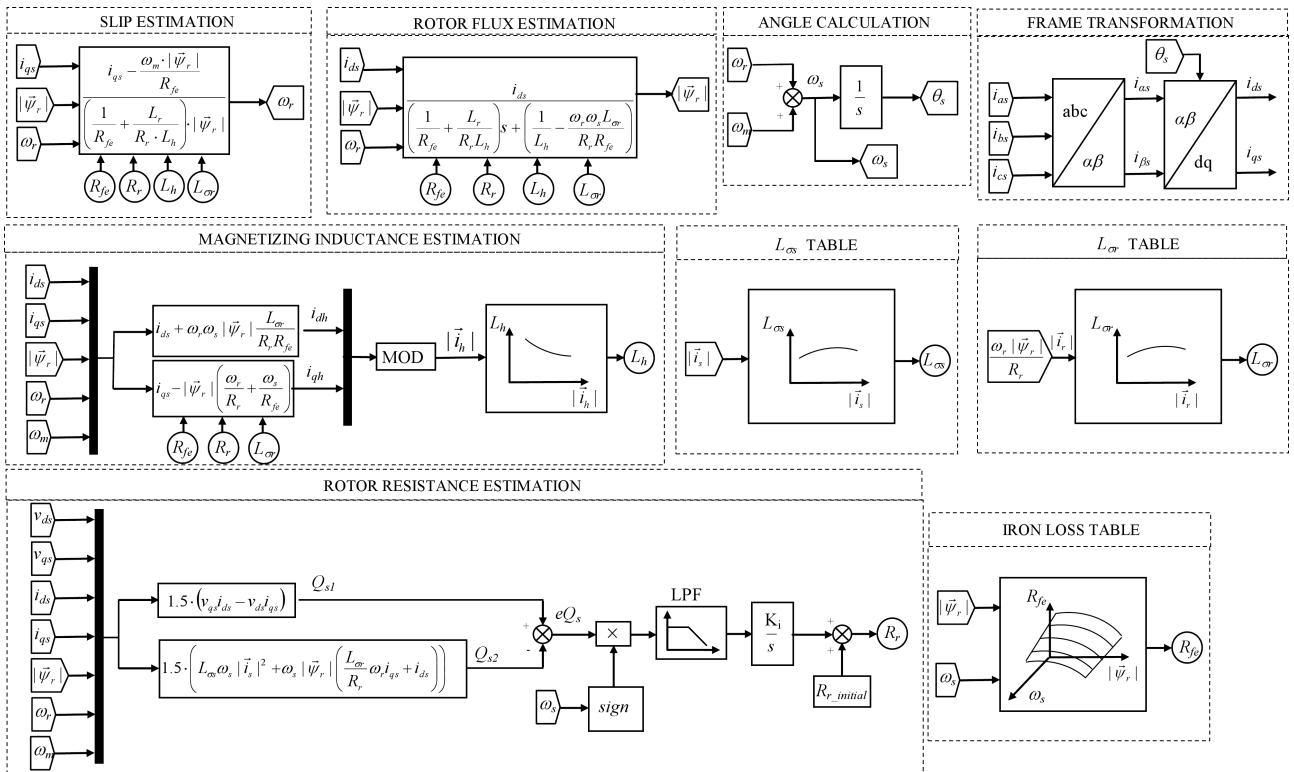


Fig. 9. Estimation block for the vector control considering the iron losses and inductances variation

In any case, the estimation structure diagram of Fig. 9 allows taking the variation of the leakage inductance into account, should it be required for a particular machine design. In this way, a well decoupled vector control strategy based on Fig. 4 can be performed, with an accurate control of torque and rotor flux amplitude. From the estimated magnitudes, the torque can be also calculated according to the following expression:

$$T_{em} = 1.5 \cdot p \cdot |\vec{\psi}_r|^2 \frac{\omega_r}{R_r}. \quad (22)$$

4. Off-line estimation of the induction machine parameters

This section describes three simple off-line tests that identify the machine parameters required by the vector control strategy. Most of the details of the tests described ion, are well known basics already covered in specialized literature as for instance [15] and [28]. The tests are very suitable for most motor-drive applications since they do not need any special modification in the system, such as a rotor locking requirement, special voltage supply or special measurements.

The off-line tests are performed with the same machine, converter and control system that will then be used in the real application. In this paper, the tests are carried out in a 15 kW-380 V-1500 rev/min IM. The control strategy is implemented in a dSPACE 1103 control board. The test bench is composed by the IM and a DC machine (load). A torque sensor is mounted at the coupling point of the axis of both machines, in order to evaluate the error on the estimated torque (Fig. 10). The Voltage Source Converter (VSC) that supplies the IM is build using 1200 V/500 A Semikrom Insulated Gate Bipolar Transistors (IGBTs), it is connected to the 380 V AC grid by using a six-pulse Diode Front End (DFE). The switching frequency of the VSC is set to 4 kHz.

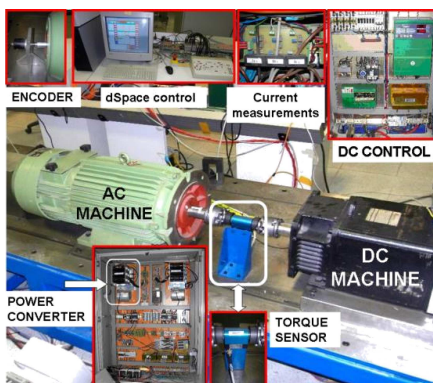


Fig. 10. Experimental platform of 15 kW IM

4.1. Stator resistance estimation test. The stator resistance R_s is estimated first. Although not strictly needed by the vector control strategy; its value will be required in the two subsequent off-line tests. In this test, the machine is fed with a DC voltage, generated by the voltage source converter as illustrated in Fig. 11. Once that steady state operation has been reached, the DC voltage will create a DC current that flows though the stator resistance. In addition, the speed of the machine will be zero, since no torque is created.

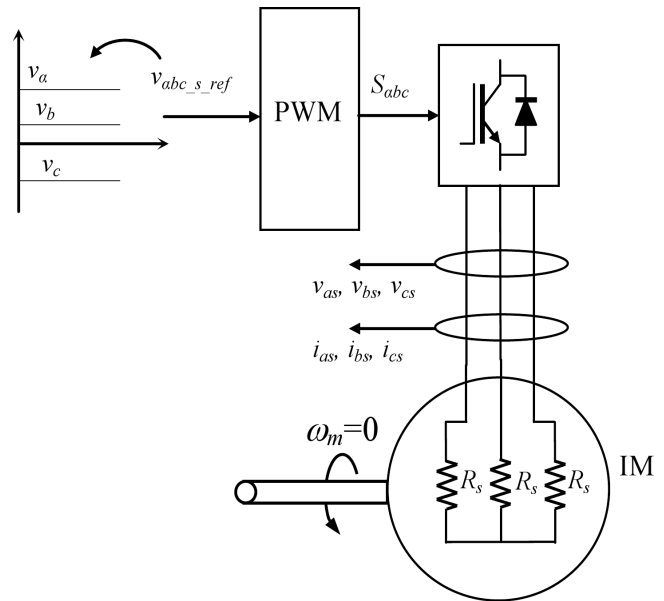


Fig. 11. Converter based stator resistance estimation

The stator resistance is then obtained by dividing the voltage applied to the stator by the current that is produced. The applied stator voltage can be either measured or assumed to be equal as its reference value. If the latter is used, all the non-linear effects of the converter such as dead-times, voltage drops in the switches, etc, should be compensated for an accurate R_s estimation. The measurements results for a current sweep performed on the test-bench machine are shown in Fig. 12. Looking at the results, a constant value of 161 mΩ has been chosen as the stator resistance R_s .

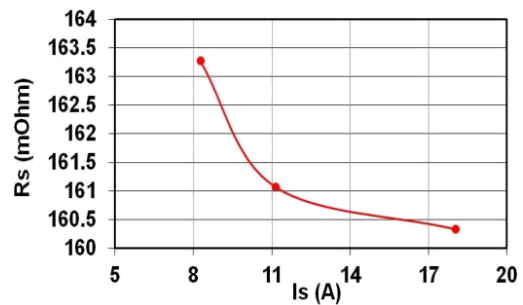


Fig. 12. Estimated stator resistance

4.2. Rotor resistance and leakage inductances estimation test. Once the stator resistance has been estimated, the next task is to estimate the rotor resistance and the leakage inductances [28]. The test is also performed at zero speed and is based on the classical rotor locked test or also known, as short circuit test. In order to avoid the need for mechanically locking the rotor axis, only two phases of the machine are fed with AC voltages, while in the third phase is left unconnected. This is equivalent to disabling one of the three converter legs of the VSC as shown in Fig. 13. In this way, since the current only flows through two windings of the machine, no torque is generated as there is no rotating magnetic field.

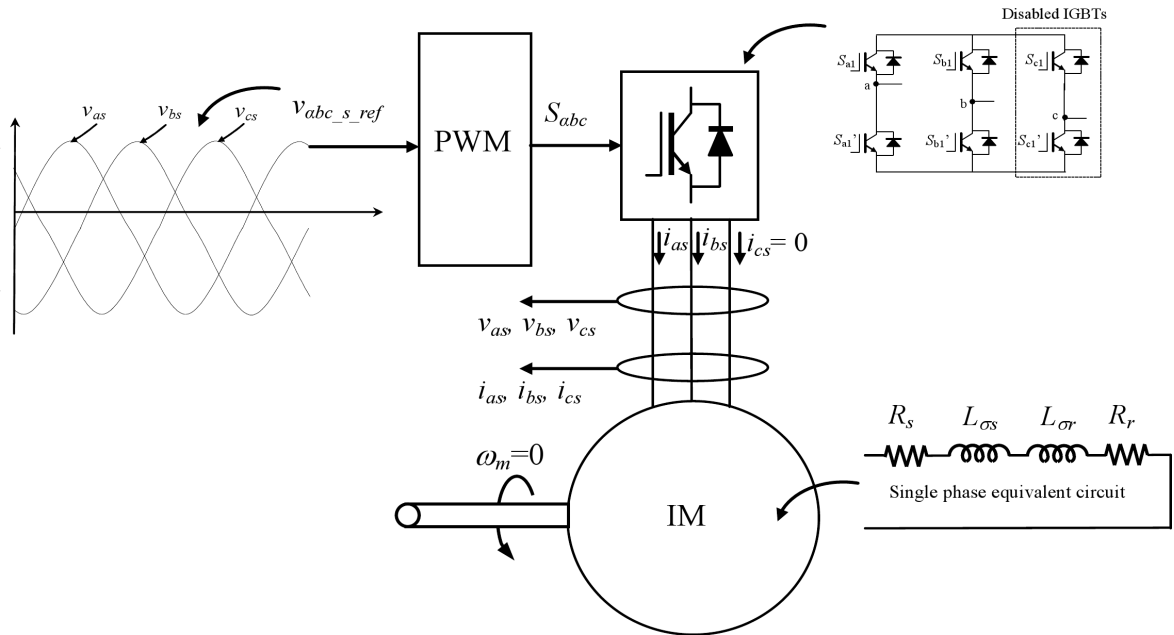


Fig. 13. Converter based rotor resistance and leakage inductances estimation

Therefore, in each winding of the machine, no current will flow through the mutual circuit (L_h and R_{fe}) since the easier path for the current at zero speed will be the rotor path. Consequently, the equivalent circuit of each of the two supplied phases will be composed of three unknown parameters; $L_{\sigma s}$, $L_{\sigma r}$ and R_r as depicted in Fig. 13. For simplicity, as suggested in [28], both stator and rotor leakage inductances are considered equal: $L_{\sigma} = L_{\sigma s} = L_{\sigma r}$. This fact yields us to now only address the off-line estimation of two unknown parameters: L_{σ} and R_r . Consequently, by feeding the stator at different amplitude and frequency voltages, it is possible to derive the parameters of Fig. 14 for the tested IM. Both parameters can be obtained from measurement of stator active, reactive powers and currents and equations:

$$R_s + R_r = \frac{P_{AC}}{2|I_{AC}|^2}, \quad L_{\sigma s} + L_{\sigma r} = \frac{Q_{AC}}{2\omega_s|I_{AC}|^2}. \quad (23)$$

Note that the measurements are assumed to be of two phases. The leakage inductances present almost constant behavior depending on the frequency and current amplitude for the tested machine. On the other hand, the estimated resistances present higher values at higher frequencies, since the rotor resistance takes higher value due to skin effects [15]. However, since the rotor resistance is estimated on-line, as explained in Subsec. 3.6, only an initial approximation is required at this point. By looking at Fig. 14, the initial value for the rotor resistance has been chosen to be $R_{r_initial} = 0.188 \Omega$, which corresponds to the test at 5 Hz at highest current amplitude ($R_s + R_r = 0.349 \Omega$). In addition, the value for the leakage inductance, which will be kept constant in this case, has a value of $L_{\sigma} = 0.003 \text{ H}$, that is, half the average value of 0.006 H shown in Fig. 14. For a different machine design, in which the leakage inductance may vary significantly depending on the operating point, the use

of look-up tables could be considered at the control stage, as proposed in Fig. 9.

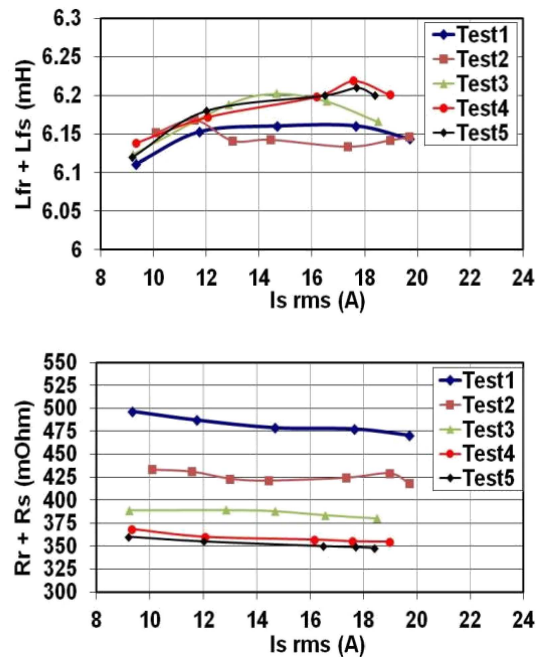


Fig. 14. Estimated leakage inductances and stator + rotor resistances. Test1: $f = 50 \text{ Hz}$, Test2: $f = 33 \text{ Hz}$, Test3: $f = 25 \text{ Hz}$, Test4: $f = 15 \text{ Hz}$, Test5: $f = 5 \text{ Hz}$

4.3. Magnetizing inductance and iron losses estimation test.

Finally the no load test provides the last two unknown parameters; L_h and R_{fe} . In this case, the machine is fed as illustrated in Fig. 15. It is controlled by the vector control proposed in Sec. 3 to different speeds and rotor flux ampli-

tude values. Since R_{fe} is unknown in this test, a very high value is set in order to disable its effect in the control. On the other hand, the other unknown value L_h is set to reasonable approximated value deduced for instance from the nameplate data provided by the manufacturer. Thus, from typically given rated values of: voltage (V_{rated}), output power (P_{rated}), power factor ($\cos\theta_{rated}$), and frequency (f_{rated}), the magnetizing inductance can be approximated, neglecting the stator resistance and leakage inductances:

$$L_h \cong \frac{\sqrt{3}V_{rated}^2}{P_{rated} \tan(\theta_{rated}) 2\pi f_{rated}}. \quad (24)$$

This uncertainty is not a problem for this no-load test, as even if a poor flux orientation is achieved, the current limit of the machine is unlikely to be reached.

For this test, a set of currents of a controlled magnitude are produced by the inverter. Based on the stator voltage and power measurements, and using the machine parameters calculated so far, the magnetizing inductance and the iron and mechanical losses can be calculated according to the mathematical calculations graphically illustrated in Fig. 13.

The results for this test are illustrated in Fig. 17., where the top plot shows the variation of the iron loss equivalent resistor against the rotor flux expressed in per-unit terms, and the bottom curve shows the variation of the magnetizing inductance against the i_h current. Therefore, these tables are implemented in the corresponding proposed estimators of Fig. 9. For the R_{fe} a three dimensional table is implemented according to Fig. 17, while for L_h a two dimensional table is sufficient. Note that the purpose of the L_h and R_{fe} estimators, is to deduce the actual operating point of the machine ($|\vec{\psi}_r|$, $|\vec{i}_h|$ and ω_s), for the mapping of these two look-up tables. Basically, the speed, the torque (by ω_r as seen in Eq. (17)) and the rotor flux (by $|\vec{i}_h|$ as seen in Eqs. (13) and (14)) influence on the R_{fe} and L_h steady-state values. Finally note that as explained in Subsec. 3.5 the mechanical losses are included and considered as iron losses.

On the other hand, since these parameters are dependent on the operating point of the machine, it is important that this test is carried out close to the operating conditions of the application. For instance producing the same stator voltage is mandatory for a good estimation of the iron losses.

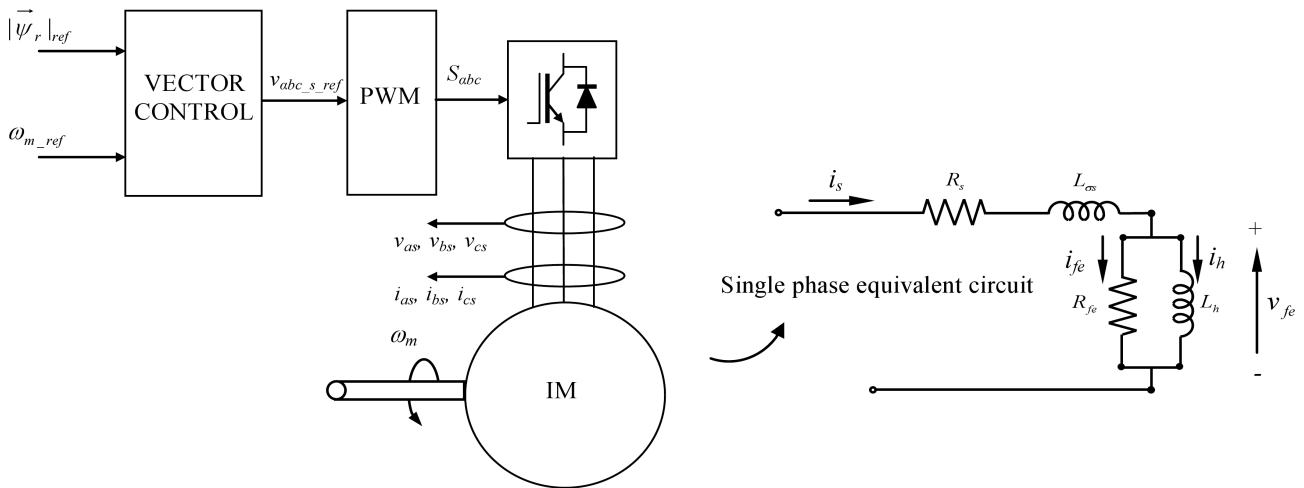


Fig. 15. Vector control based no-load test

$$\left. \begin{array}{l} \underline{I}_s \quad P_s \\ \underline{V}_s \quad Q_s \end{array} \right\} \Rightarrow \left. \begin{array}{l} P_{fe} = P_s - P_{R_s} \\ P_{R_s} = 3 \cdot |\underline{I}_s|^2 \cdot R_s \\ \underline{V}_{fe} = \underline{V}_s - (R_s + j \cdot \omega_s \cdot L_{\sigma s}) \cdot \underline{I}_s \\ Q_{L_h} = Q_s - 3 \cdot \omega_s \cdot L_{\sigma s} \cdot |\underline{I}_s|^2 \end{array} \right\} \Rightarrow \left. \begin{array}{l} R_{fe} = \frac{3 \cdot |\underline{V}_{fe}|^2}{P_{fe}} \\ L_h = 3 \cdot \frac{|\underline{V}_{fe}|^2}{\omega_s \cdot Q_{L_h}} \end{array} \right\}$$

Fig. 16. L_h and R_{fe} calculation procedure, from stator current, voltage and power measurements

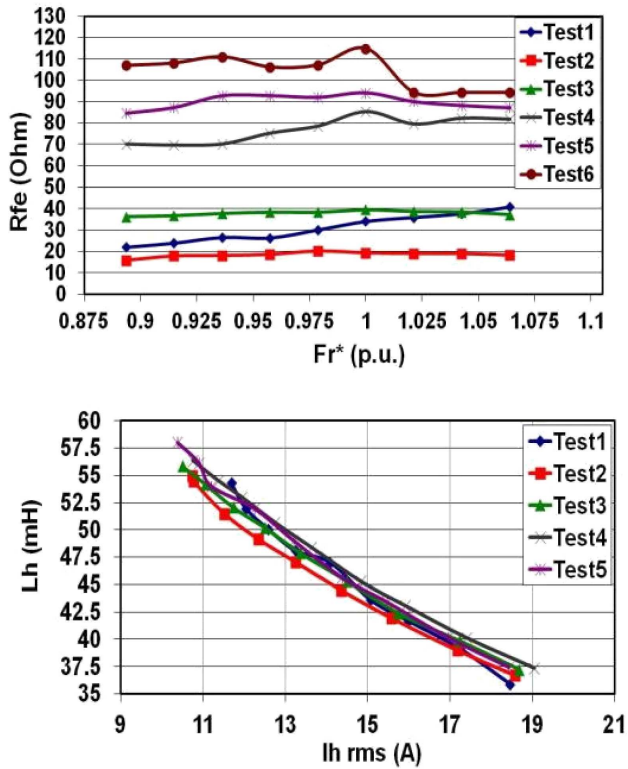


Fig. 17. Estimated iron loss resistance and magnetizing inductance, Test1: $\omega_{mec} = 0.066$ p.u., Test2: $\omega_{mec} = 0.133$ p.u., Test3: $\omega_{mec} = 0.3$ p.u., Test4: $\omega_{mec} = 0.5$ p.u., Test5: $\omega_{mec} = 0.66$ p.u

Factors such as modulation techniques, a different switching frequency, etc... can produce different iron losses behavior as illustrated in Fig. 18. It can be seen in that figure how with a pure sinusoidal voltage supply, the iron losses are significantly reduced compared to a VSC supply.

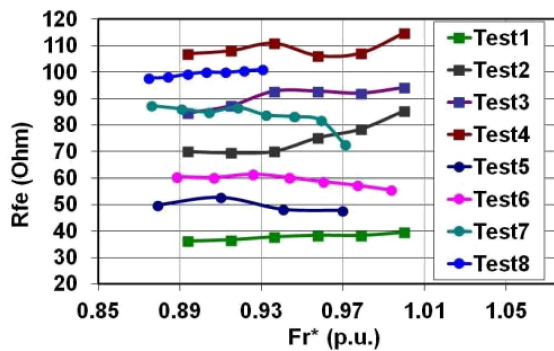


Fig. 18. Comparison of iron losses with PWM supply and sinusoidal supply at different speeds, **PWM Tests:** Test1: $\omega_{mec} = 0.3$ p.u., Test2: $\omega_{mec} = 0.5$ p.u., Test3: $\omega_{mec} = 0.66$ p.u., Test4: $\omega_{mec} = 1$ p.u.; **Sinusoidal Tests:** Test5: $\omega_{mec} = 0.3$ p.u., Test6: $\omega_{mec} = 0.5$ p.u., Test7: $\omega_{mec} = 0.66$ p.u., Test8: $\omega_{mec} = 1$ p.u

5. Experimental validation of the proposed control and testing procedure in a 15 kw experimental test bench

5.1. Preliminary evaluation. The performance of the proposed control algorithm is evaluated in the 15kW machine

presented in previous section. The objective of this experimental validation is to evaluate the improvement on the torque accuracy of the drive in a low-scale test bench when the proposed control strategy is in place, at steady-state and during transients.

The evaluation has been divided into five different experiments. The first experiment shows an improvement in the accuracy, achieved thanks to the proposed vector control strategy. In Fig. 19a, the torque error performance is shown disabling the estimators proposed in this paper to provide a benchmark to compare the improvements offered by the proposed control strategy. In that experiment, the load torque is varied keeping the flux and speed constant. The estimated torque error per-unit is then evaluated as follows:

$$eT_{em} = \frac{(T_{em})_{estimated} - (T_{em})_{sensor}}{(T_{em})_{rated}}, \quad (25)$$

where the rated electromagnetic torque for this machine is $(T_{em})_{rated} = 95$ Nm. The diamond-dotted line in the figure shows the performance using the off-line L_h and R_r estimated parameters, whereas the square-dotted and circle-dotted curves correspond to a variation of 1.35 p.u. of L_h and R_r respectively. Note that without considering the iron losses and with a short deviation of the L_h and R_r parameters from their off-line estimated values, the torque error goes easily beyond 4%. Note that the imposed parameter uncertainty is reasonably realistic, since the L_h and R_r may vary easily during the operation, due to the magnetizing level of the machine and the temperature increase. As a consequence, when the torque error is high, the system could present more difficulties to reach the nominal torque, due to a non-proper decoupling of the stator currents.

On the other hand, Fig. 19b shows the torque errors without considering the iron losses, but having the L_h and R_r estimators enabled. For that purpose, the R_{fe} is set to a very high value, while to avoid possible non-linear effects and uncertainties of the VSC, the measured stator voltages are used for the R_r estimator. The estimated torque error is somehow similar to that obtained in Fig. 19a when using the off-line measured L_h and R_r values. It can be noticed that the bigger the torque, bigger the torque error becomes.

The next part of the experiment shows the importance of the stator voltage value for the R_r estimator. Depending on the VSC used and how it has been constructed and implemented, the stator voltage reference for the VSC can be far from the real imposed stator voltage in the machine. Fig. 19c shows with square-dotted and diamond-dotted lines the torque error produced when the R_r estimator operates with reference voltages and measured voltages respectively. Consequently, it is very important to be aware of the limitations of the VSC that is used, as stator voltage sensors may be required for good torque accuracy. If for cost or simplicity reasons, the use of stator voltage sensors is not feasible, it may be crucial to compensate the non-linear effects of the VSC such as dead-times, voltage drops in the semiconductors, etc. [24].

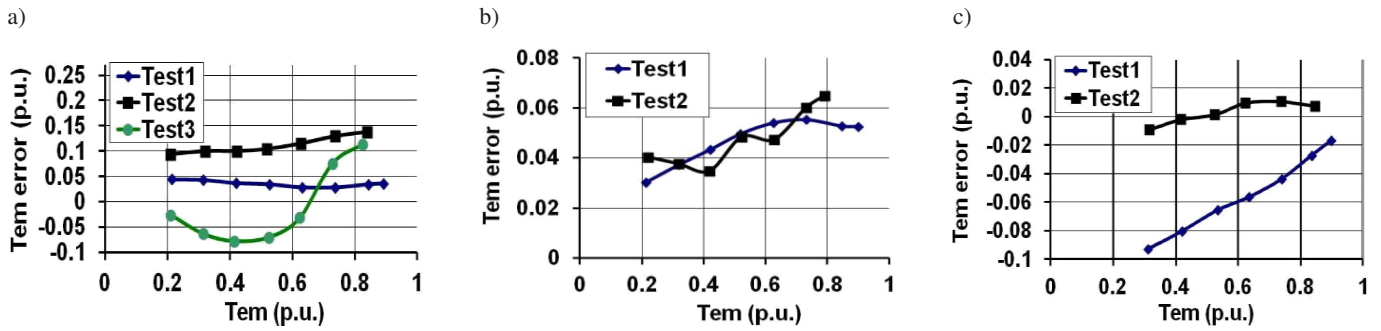


Fig. 19. Torque estimation errors at constant speed $\omega_{mec} = 0.5$ p.u., under different estimation conditions, a) torque errors with all the estimators disabled and voltage sensors at constant flux, $\psi_{*r} = 1$ p.u. Test1: $L_h = 1$ p.u., $R_r = 1$ p.u., Test2: $L_h = 1.35$ p.u., $R_r = 1$ p.u., Test3: $L_h = 1$ p.u., $R_r = 1.5$ p.u.; b) torque errors with only L_h and R_r estimators enabled (not considering the iron losses) and voltage sensors. Test1: $\psi_{*r} = 1$ p.u., Test2: $\psi_{*r} = 0.9$ p.u.; c) torque errors with all the estimators enabled with different stator voltage inputs. Test1: With stator voltage reference. Test2: With stator voltage measurement

5.2. Steady-state evaluation at different speeds. In the second experiment, the torque error is evaluated in a wide range of speeds at steady-state, against different load torque values, with the proposed complete control strategy and estimators, having also stator voltage sensors connected. Figure 20a illustrates that the achieved torque errors are within a 3% error band in all conditions, showing that the vector control achieves a good stator current decoupling thanks to the proposed es-

timators. The estimated R_r , L_h , R_{fe} and R_r values for all the operating points tested in this experiment are shown in Figs. 20b–d, and Fig. 20e respectively. It is interesting to note in Fig. 20b that regardless of the speed, the estimated value of R_r approaches the off-line measured value only for relatively high values of torque. Thus, although the proposed estimator achieves a very good torque accuracy (within 3% of error), the estimated R_r value is not accurate at lower torques.

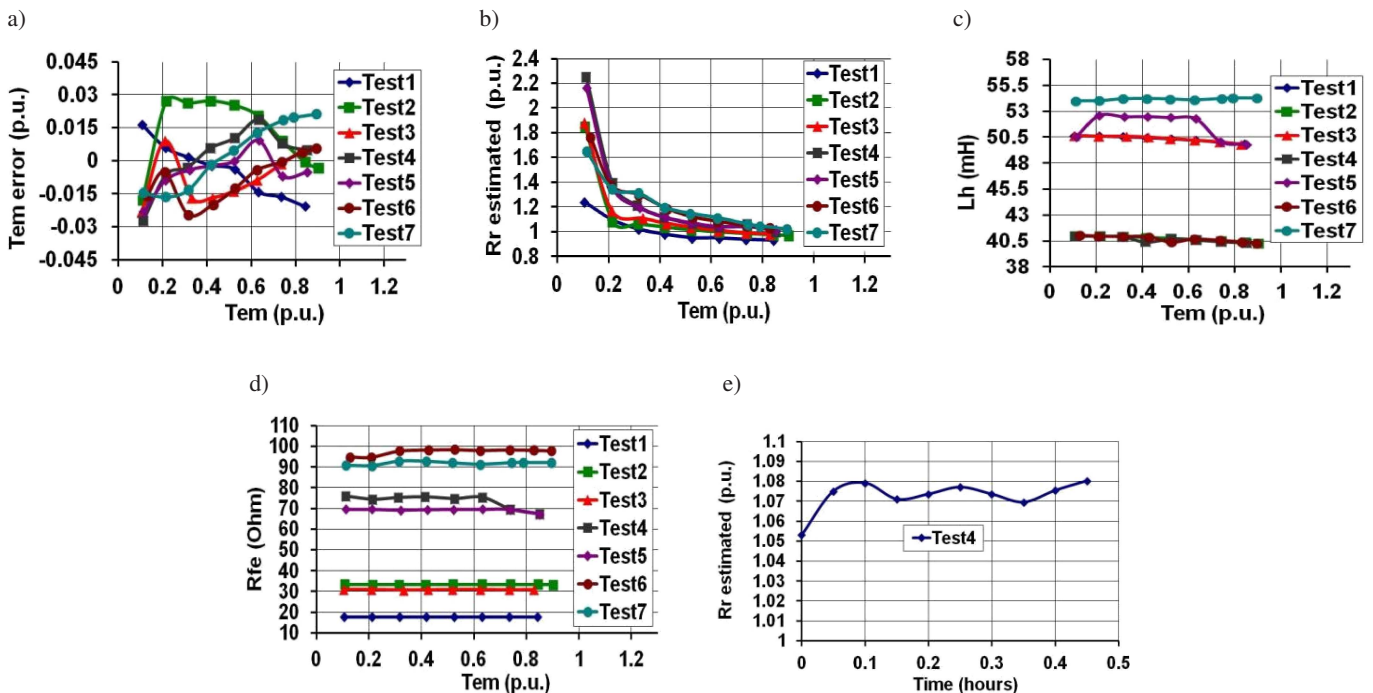


Fig. 20. Torque estimation errors and estimated parameters, at different torque and speed conditions, with all the estimators enabled. a) Torque errors, b) estimated R_r values, c) estimated L_h values, d) estimated R_{fe} values, e) estimated R_r at constant speed and torque with all estimators enabled. Test1: $\omega_{mec} = 0.13$ p.u., $\psi_{*r} = 0.915$ p.u., Test2: $\omega_{mec} = 0.25$ p.u., $\psi_{*r} = 1$ p.u., Test3: $\omega_{mec} = 0.25$ p.u., $\psi_{*r} = 0.915$ p.u., Test4: $\omega_{mec} = 0.5$ p.u., $\psi_{*r} = 1$ p.u., Test5: $\omega_{mec} = 0.5$ p.u., $\psi_{*r} = 0.915$ p.u., Test6: $\omega_{mec} = 0.75$ p.u., $\psi_{*r} = 1$ p.u., Test7: $\omega_{mec} = 0.75$ p.u., $\psi_{*r} = 0.915$ p.u.

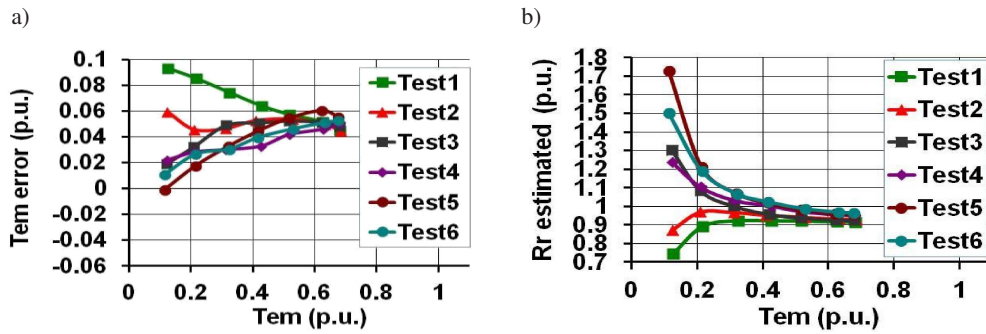


Fig. 21. Algorithm performance at different torque and speed conditions, with L_h and R_r estimators enabled but not considering the iron losses, a) torque errors, b) estimated R_r values. Test1: $\omega_{mec} = 0.25$ p.u., $\psi_{*r} = 1$ p.u., Test2: $\omega_{mec} = 0.25$ p.u., $\psi_{*r} = 0.915$ p.u., Test3: $\omega_{mec} = 0.5$ p.u., $\psi_{*r} = 1$ p.u., Test4: $\omega_{mec} = 0.5$ p.u., $\psi_{*r} = 0.915$ p.u., Test5: $\omega_{mec} = 0.75$ p.u., $\psi_{*r} = 1$ p.u., Test6: $\omega_{mec} = 0.75$ p.u., $\psi_{*r} = 0.915$ p.u.

This phenomenon can be justified as follows: non-modeled non-linearities of the machine and errors in the voltage and currents sensing affect the Q_s errors. The R_r estimator corrects these Q_s errors, estimating a slightly different value of R_r from its actual value, providing accurate torque estimation. Note that the estimated R_r variation from its off-line estimated value is more severely affected at lower torques (up to $R_r = 2.25$ p.u.). Nevertheless, from Eq. (20) is deduced that at low torques (low i_{qs}), the influence of the R_r is very low to correct the Q_s errors in the estimator, yielding to a high resistance variation to correct small Q_s errors. This fact, in practical solutions, could lead to disabling of the rotor resistance estimator at low torques (0.25 p.u. for instance), without producing a significant torque accuracy degradation.

In addition, It can be noticed by looking at Fig. 20c, which shows the estimated L_h value for each of the tested operating conditions in the experiment, that the magnetizing inductance L_h value is higher for lower rotor flux levels as expected. It must be highlighted that it is also very important to know the actual value of this parameter, otherwise, the torque estimation can be dramatically deteriorated (check Fig. 19a for instance).

On the other hand, Fig. 20d shows how the estimated R_{fe} value is affected by both the speed and rotor flux level, exhibiting the predicted trend. This variation be more or less important, depending on the iron loss performance characteristic of the machine under controlled.

Finally, the last part of this experiment illustrates the estimated R_r value at constant speed (0.5 in p.u.) and torque (0.63 in p.u.). Figure 20e illustrates that after some time, it settles to a stable value as the machine temperature reaches a steady state value.

In contrast, Fig. 21 illustrates the performance of the algorithm without considering the iron losses (setting $R_{fe} \rightarrow \infty$ in the estimators of Fig. 9), but, unlike in Fig. 19a, using the actual stator voltage provided by voltage sensors. In this way,

as seen in Fig. 21a, the torque accuracy is deteriorated from previous evaluation (considering R_{fe}). On the other hand, the estimated R_r presents similar behavior as previous evaluation, but with a perhaps smaller variation from its off-line estimated value.

5.3. Steady-state evaluation with flux weakening. The next test presented in this Section evaluates the proposed control operating in the flux weakening region. For that purpose the speed of the machine is maintained constant to the rated value, while the torque error is evaluated at different rotor flux amplitude levels. Thus, Fig. 22 illustrates the results for this test, where the measurements were taken once the machine had reached a steady-state operation. Figure 22a shows the torque error against different values for electromagnetic torque. As seen in the previous experiments, the consideration of the iron losses provides reasonably good torque results at different flux levels.

Again, the estimated R_r presents a similar trend to that observed in previous experiments, exhibiting a tendency to estimate lower R_r values at lower fluxes.

On the other hand, the estimated value of the magnetizing inductance L_h , shown in Fig. 22c, also varies for different flux levels as expected. The importance of the L_h estimator must be highlighted again, in order to achieve a good torque accuracy.

Finally, the estimated R_{fe} exhibits also a tendency to vary its value depending on the flux level, as predicted theoretically. Consequently, these tests indicate that both L_h and R_{fe} together with the R_r estimator are necessary tools to achieve reasonably good torque performance. To conclude with this experiment, Fig. 22e shows experimental waveforms, captured using the proposed control strategy, for the stator voltage (top waveform), stator current (mid waveform) and torque demand (bottom waveform) during a step in the torque demand.

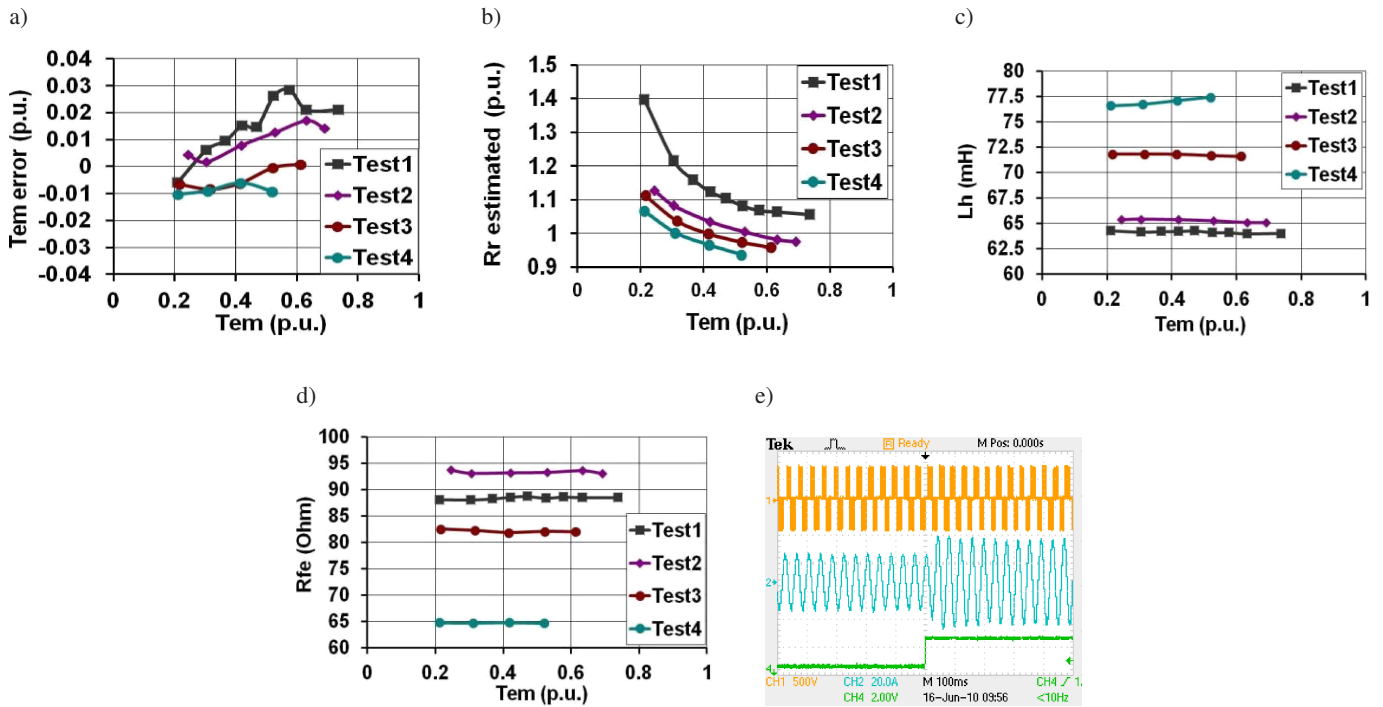


Fig. 22. Torque estimation errors and estimated R_r , at different torque and fluxes (nominal speed conditions) with all the estimators enabled. (a) Torque errors, (b) Estimated R_r values, (c) Estimated L_h values, (d) Estimated R_{fe} values, (e) Oscilloscope captures of stator voltage for phase A, top waveform, 500 V/div, and phase A current, mid-waveform, 20 A/div, for the proposed control strategy during a torque step, bottom waveform. 100 ms/div. Test1: $\psi^*_{*r} = 0.85$ p.u., Test2: $\psi^*_{*r} = 0.78$ p.u., Test3: $\psi^*_{*r} = 0.70$ p.u., Test4: $\psi^*_{*r} = 0.57$ p.u.

5.4. Performance during transients. In the previous section, the proposed control strategy has shown to offer an improved performance and torque accuracy at steady state operation. In this section, the performance of this new strategy is evaluated for transient operation. In the two previous subsections, it has been seen that the R_r estimator reaches a different value depending on mainly three variables: torque, speed and rotor flux (Fig. 20b and Fig. 22b). In addition, this estimator needs a settling time to reach its steady-state final value. Consequently, the dynamic performance of the estimator, determined by the gain K_i of the integrator, as seen in Fig. 5, compromises the dynamic performance of the overall system. Note that the rest of the estimators (L_h and R_{fe}) do not present this slow dynamic stabilization.

Consequently, the transient performance is evaluated as follows:

- Torque load steps are performed with the DC machine, while the speed regulator of the AC machine is tuned so the speed is not affected by the load torque variation. In this way, the machine goes from one point of any other curve of Fig. 20 to other point of the same curve straight away, without giving the R_r estimated value time to change.
- The integrator constant of the R_r estimator, K_i , is set to different values, each of those achieving different estimation speeds of R_r , which achieve an eventual elimination of the torque error with different speeds.
- Under this situation, the torque error is evaluated according to Eq. (22) and recorded.
- The performance of the proposed control algorithm is com-

pared, with that of a control control strategy that does not consider the iron losses (R_{fe} set to a very high value).

Thus, Fig. 23 shows the results for the dynamic performance comparison with torque steps from 0.3 to 0.65 p.u. In Figs. 23a,b and c show the estimated torque error, the variation of R_r and the variation of the Q_s error respectively. These figures show that the smaller K_i is, the more time is needed to eliminate the Q_s error and consequently, more time is also needed to reach the steady-state and minimize the torque errors. Note that while the new torque level is reached in very little time, since the new R_r estimation requires some seconds to find its good value, the torque error needs also some seconds to be minimized. Unfortunately, it is not advisable to accelerate the estimation R_r process too much, which was initially devised to compensate slow temperature drift variations of the rotor resistance, as this could bring instability.

On the other hand, under the same conditions but disabling the iron losses estimation, the performed tests show a slightly faster dynamic response than the complete control. As exhibited in Figs. 23d–f, equivalent to Figs. 23a–c but without considering iron losses, both the R_r and the torque present shorter settling times. However, the torque error is greater.

Consequently, it can be concluded that the proposed control algorithm requires larger R_r variations in the estimation, during transients but the resulting torque error is smaller. On the contrary, if the torque step is performed at a operating point where none of the controls require a large R_r variation (above 0.5 p.u. for instance), the dynamic performance of the R_r and torque errors become very similar.

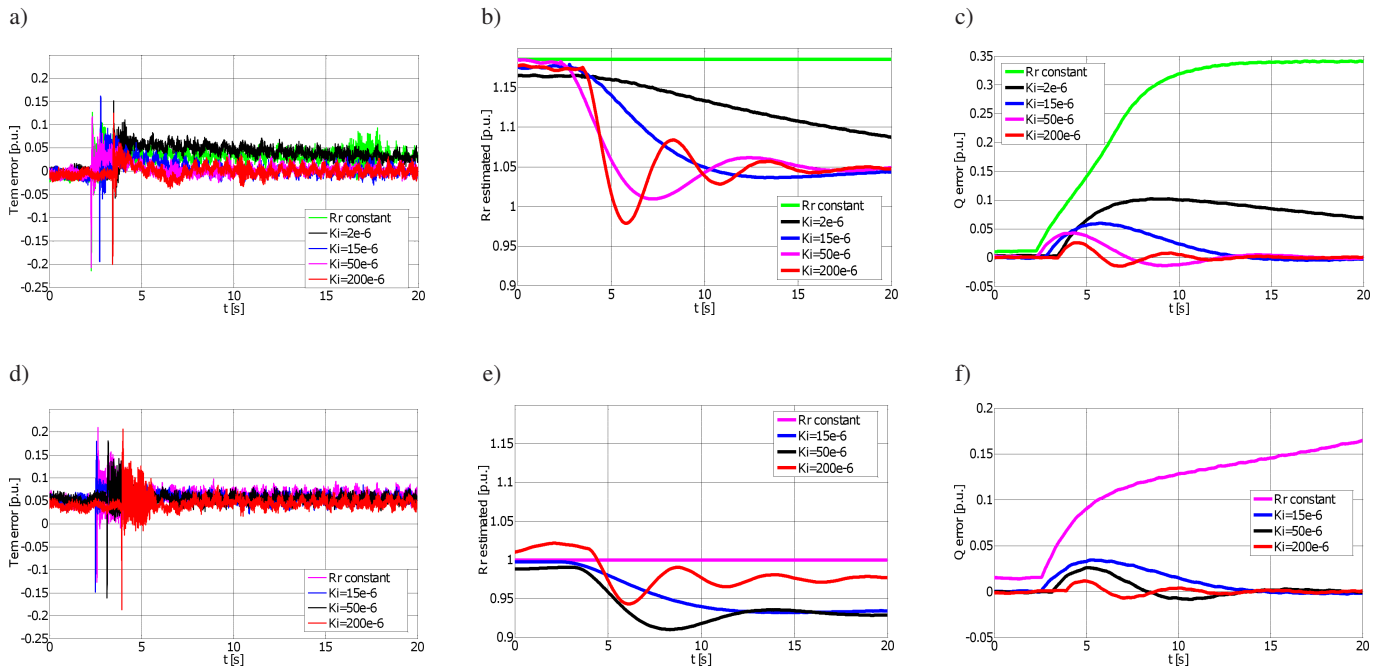


Fig. 23. Dynamic performance of the estimation at different K_i values of the R_r estimator, under torque steps from 0.3 to 0.65 p.u. a) torque errors with the proposed algorithm, b) estimated R_r with the proposed algorithm, c) Q_s errors with the proposed algorithm, d) torque errors without considering the iron loss, e) estimated R_r without considering the iron loss, f) Q_s errors without considering the iron loss

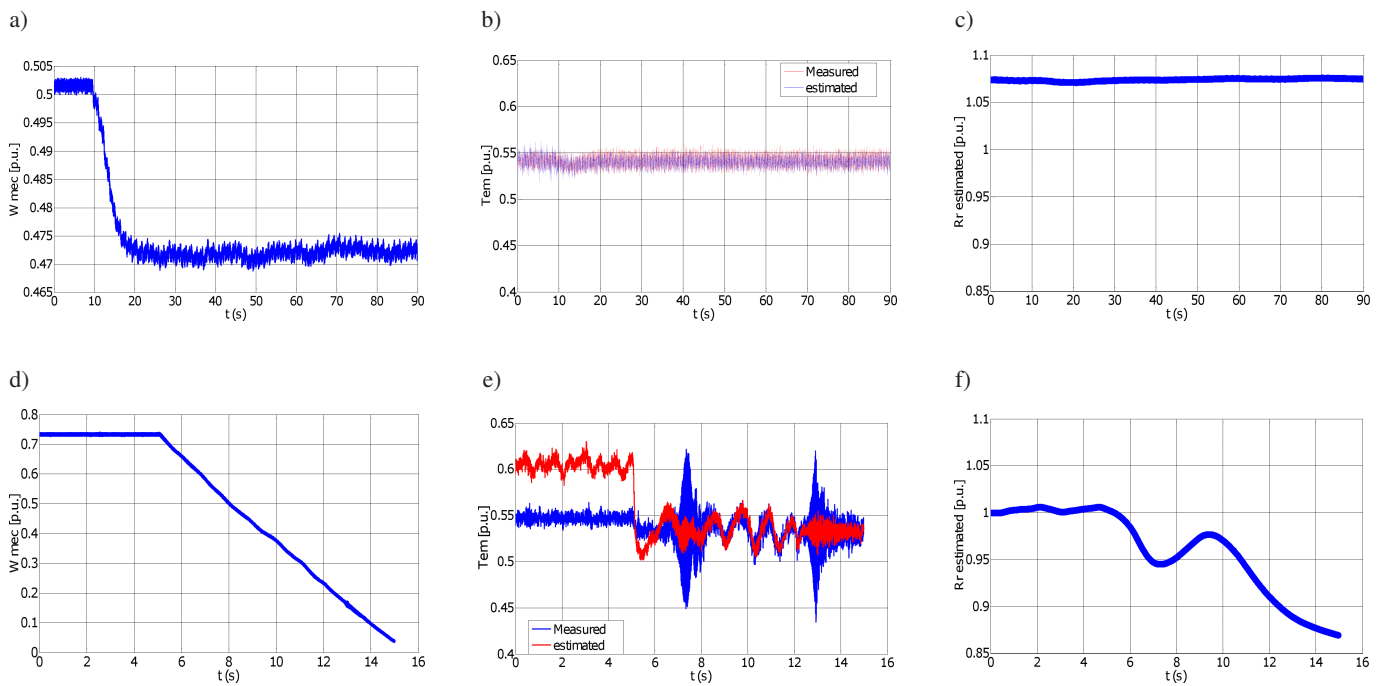


Fig. 24. Performance disabling the speed sensor, (a, b and c with all estimators enabled and d, e and f with iron losses estimator disabled), a) speed, b) torque performance, c) R_r estimation, d) speed, e) torque performance, f) R_r estimation

5.5. Performance without speed control. The last set of experiments was done by having both DC and AC machines controlled in torque, with the speed control disabled. The experiment procedure is described as follows:

1. By enabling the speed regulator of the AC machine, the system is driven to a 0.5 p.u. constant speed.
2. The torque of the DC machine is set to a constant value (the AC machine sees approximately that torque load).
3. The speed regulator of the AC machine is disabled and the torque capture of the torque sensor is provided as the torque reference of the AC machine ($T_{em.ref}$ in Fig. 4). After a given time, the speed regulator is disabled and the torque measurement becomes the torque reference of the AC machine, producing a short speed transient that gets stabilized after few seconds.

Figure 24 illustrates how a stable performance of the system is only achieved for the control strategy that has all the estimators enabled (Figs. 24a, b and c), where the speed regulator is disabled after 10 seconds of operation.

On the contrary, the control that does not consider the iron losses of the machine, due to its worse torque estimation accuracy, provokes a quick speed drift and unstable behavior (Figs. 24d, e and f). Note that the speed regulator is disabled after 5 seconds in this case.

5.6. Performance of different power machines. Finally, this last section evaluates the effectiveness of the proposed control algorithm that considers the iron losses, in machines of different nature. For this purpose, the X_h/R_{fe} ratio is proposed as a simple indicator to evaluate the relevance of the iron losses in a given machine. Table 1 [5] serves as an illustrative example of this ratio (at rated frequency), in machines of different power, voltage and pair of poles.

Table 1
Different machine's characteristics

P_s [kW]	X_h/R_{fe}	Voltage [V]	Poles
15	0.136	380	4
180	0.085	380	4
3250	0.057	690	6
4000	0.037	690	6
4000	0.038	6600	4
4000	0.024	6600	6
4000	0.022	6600	8

By looking at the table, it can be concluded that for machines of a rated power greater than a few dozens of kW, the iron losses become less significant, being possible to neglect them at the control stage, without expecting a significant degradation of the torque control accuracy. This is in good agreement with previous work by other authors [22].

6. Conclusions

This research work has proposed a drive oriented vector control strategy in which its novelty consists on the consideration of all the variation of the machine parameters due to

the normal operation, including also the iron losses. Thanks to this proposed parameter adaptation philosophy, accurate torque control can be obtained as demanded in many industrial applications.

For that purpose, a set of different on-line operating machine parameter estimators have been studied. Most of these estimators require information obtained in a series of off-line tests. A set of tests based on classic AC machines knowledge have been carried out, not requiring any special power source or extra mechanism to perform them. This fact is advantageous for the commissioning of the drive in a real application. Especially, when information supplied by the manufacturer of the machine is not available or is incomplete. These tests can be easily implemented in a self-commissioning automated process.

The experimental validation has revealed the effectiveness of the proposed control strategy and estimators as well as the off-line tests. This effectiveness has been widely evaluated in terms of accurate torque estimation at steady-state and under transients. The iron losses consideration by the control has shown to be a key factor to reach torque accuracies lower than 3%. In machines of power greater than 100 kW it is expected that its influence is less significant.

The new control can be easily implemented, with very little added complexity to that of classic vector control schemes, whilst allowing the possibility of disabling any of the estimators, should the machine control require it.

REFERENCES

- [1] F. Blaschke, "A new method for the structural decoupling of A.C. induction machines", *Conf. Rec. IFAC 1*, CD-ROM (1971).
- [2] W. Leonhard, *Control of Electrical Drives*, Springer-Verlag, Berlin, 1985.
- [3] B.K. Bose, "Power electronics and motor drives recent progress and perspective", *IEEE Trans. Industrial Electronics* 56, 581–588 (2009).
- [4] H.N. Hickok, "Adjustable Speed – A Tool for saving energy losses in pumps, fans, blowers, and compressors", *IEEE Trans. on Industry Applications* IA-21, 124–136 (1985).
- [5] <http://www.ingeteam.com>
- [6] S. Kouro, M. Malinowski, K. Gopakumar, J. Pou, L.G. Franquelo, B. Wu, J. Rodriguez, M.A. Pérez, and J.I. Leon, "Recent advances and industrial applications of multilevel converters", *IEEE Trans. on Industrial Electronics* 57 (8), 2553–2580 (2010).
- [7] F. Bonnet, P.E. Vidal, and M. Pietrzak-David, "Direct torque control of doubly fed induction machine", *Bull. Pol. Ac.: Tech.* 54 (3), 307–314 (2006).
- [8] I. Takahashi and Y. Ohmori, "High-performance direct torque control of an induction motor", *IEEE Trans. Ind. Applicat.* 25, 257–264 (1989).
- [9] M. Depenbrock, "Direct self-control (DSC) of inverter-fed induction machine", *IEEE Trans. Power Electron.* 3, 420–429 (1988).
- [10] P. Antoniewicz and M.P. Kazmierkowski, "Predictive direct power control of three phase boost rectifier", *Bull. Pol. Ac.: Tech.* 54 (3), 287–292 (2006).

- [11] D. Casadei, G. Serra, A. Tani, and L. Zarri, "Assessment of direct torque for induction motor drives", *Bull. Pol. Ac.: Tech.* 54 (3), 237–254 (2006).
- [12] E. Levi, "Impact of cross-saturation on accuracy of saturated induction machine models", *IEEE Trans. on Energy Conversion* 12 (3), 211–216 (1997).
- [13] R.C. Healey, S. Williamson, and A.C. Smith, "Improved cage rotor models for vector controlled induction motors", *IEEE Trans. on Industry Applications* 31 (4), CD-ROM (1995).
- [14] A.C. Smith, R.C. Healey, and S. Williamson, "A transient induction motor model including saturation and deep bar effect", *IEEE Trans. on Energy Conversion* 11 (1), CD-ROM (1996).
- [15] I. Boldea and A. Nasar, *The Induction Machine Handbook*, CRC Press, London, 2001.
- [16] S. Maiti, C. Chakraborty, Y. Hori, and Minh C. Ta, "Model reference adaptive controller-based rotor resistance and speed estimation techniques for vector controlled induction motor drive utilizing reactive power", *IEEE Trans. on Industrial Electronics* 55 (2), CD-ROM (2008).
- [17] P. Roncero, A. García, and V. Feliu, "Rotor-resistance estimation for induction machines with indirect-field orientation", *Elsevier Control Engineering Practice* 15 (9), 1119–1133 (2007).
- [18] S. Wade, M.W. Dunnigan, and B.W. Williams, "A new method of rotor resistance estimation for vector-controlled induction machines", *IEEE Trans. on Industrial Electronics* 44 (2), CD-ROM (1997).
- [19] J. Faiz and M.B.B. Sharifian, "Different techniques for real time estimation of an induction motor rotor resistance in sensorless direct torque control for electric vehicle", *IEEE Trans. on Energy Conversion* 16 (1), 1045–1053 (2001).
- [20] E. Levi and S.N. Vukosavic, "Identification of the magnetising curve during commissioning of a rotor flux oriented induction machine", *IEE Proc. on Electric Power Applications* 146 (6), CD-ROM (1999).
- [21] E. Levi, "Impact of iron loss on behaviour of vector controlled induction machines", *IEEE Trans. on Industry Applications* 31 (6), 1287–1296 (1995).
- [22] E. Levi, M. Sokola, A. Boglietti, and M. Pastorelli, "Iron loss in rotor flux oriented induction machines: identification, assessment of detuning and compensation", *IEEE Trans. on Power Electronics* 11 (5), 698–709 1996.
- [23] J. Holtz, "Sensorless control of induction machines – with or without signal injection?", *IEEE Trans. on Ind. Electronics* 53 (1), 7–30 (2006).
- [24] M. Hinkkanen, L. Harnefors, and J. Luomi, "Reduced-order flux observers with stator-resistance adaptation for speed-sensorless induction motor drives", *IEEE Trans. Power Electron* 25 (5), 1173–1183 (2010).
- [25] J. Holtz, J. Quan, "Drift and parameter compensated flux estimator for persistent zero stator frequency operation of sensorless controlled induction motors", *IEEE Trans. Ind. Appl.* 39 (4), 1052–1060 (2003).
- [26] S. Beineke, F. Schutte, and H. Grotstolen, "Comparison of methods for state estimation and on-line identification and position control loops", *Proc. Eur. Power Electronics Conf. EPE 1997* 3, 3.364–3.369 (1997).
- [27] H. Rasmuse, M. Kundsén, and M. Tonnes, "Parameter estimation of inverter and motor model at standstill using measured current only", *IEEE Trans. on Industrial Electronics* 46 (1), 139–149 (1999).
- [28] Institute of Electrical and Electronics Engineers (IEEE), *IEEE Standard Procedure for Polyphase Induction Motors and Generators*, *IEEE Standard 112–1996*, IEEE Press, New York, 1996.